Minimizing wave propagation dispersion by optimal parameter search in mimetic finite differences.

Miguel Ferrer

ABSTRACT

The discrete nature of the numerical operators used in wave propagation leads to dispersion errors in the simulation. The effects of dispersion can be mitigated by resorting to high-order operators, which yield more precise results at a greater computational cost. The mimetic finite-difference method introduced by Castillo et al. consists of finite-difference operators that retain a high order of accuracy when tackling Dirichlet boundary conditions, such as the free-surface condition in onshore acquisitions. The mimetic operators can be constructed by adjusting six free parameters. I present a study of the impact that varying the parameters has on the dispersion of a wave propagating in a 1-D medium, while looking for the optimal combination to minimize the numerical error at no increased computation cost.

INTRODUCTION

One of the most ubiquitous problems in geophysical imaging is simulating the propagation of seismic waves through the Earth's crust. Seismic waves enable us to compose images of the upper layers of the earth by providing information about the structures that lie beneath the surface. The wave propagation should be modeled as accurately as possible to obtain images that better represent the underlying geology.

More often than not, an analytical solution to the wave equation cannot be found because of the complexity of the simulation; and thus, we favor numerical approximations. The accuracy of the approximated solution is determined, among other factors, by the order of the numerical method used. A higher-order method yields results with reduced dispersion compared to its lower-order counterpart, often at the expense of increased computing cost.

The most prevalent method in seismic modeling is the Finite-Difference (FD) method because of its simplicity. Moreover, the FD operator can be designed in a straightforward manner for a desired order of accuracy, and it is easy to optimize compared to other methods. Nevertheless, this method has some downsides: high-order FD operators struggle to incorporate solutions with Dirichlet boundary conditions with accuracy, as well as to deal with irregularly-shaped domains—for instance, when including faults or surfaces with topographic features.

Onshore seismic simulations typically include a free-surface Dirichlet boundary condition to represent the tractionless interface between ground and air. On the surface, the wave does not exert traction in the vertical direction. By incorporating this condition, we introduce in our simulation surface phenomena, such as Rayleigh and Love waves, that need to be accurately modeled.

To model the free-surface condition without compromising the precision of our results, we use a class of FD operators called the Mimetic Finite-Difference (MFD) operators (Castillo et al. (2001)). The MFD method defines two operators that preserve the order of accuracy when Dirichlet boundary conditions are present. The MFD operators can be constructed from a set of three parameters for each operator.

The present work constitutes a study of the effect of varying the parameters when constructing the MFD operators, for the 1-D case. In particular, I analyze the impact that different MFD operators have on the dispersion of elastic waves in the presence of a free-surface condition, while searching for an optimal set of parameters to minimize numerical dispersion in the 1-D case.

ELASTIC WAVE PROPAGATION USING MIMETIC FINITE-DIFFERENCE OPERATORS

The velocity-stress formulation of the elastic equation is a system of coupled differential equations. For the 1-D, isotropic case, the system can be described as follows:

$$\begin{aligned} \rho \frac{\partial v_x}{\partial t} &= \frac{\partial \sigma_{xx}}{\partial x} + F_x(t) \\ \frac{\partial \sigma_{xx}}{\partial t} &= (\lambda + 2\mu)\, \frac{\partial v_x}{\partial x}, \end{aligned} \tag{1}$$

where ρ is the density of the medium, v_x represents the velocity component, σ_{xx} represents the compressional stress, $F_x(t)$ is the force originating the wave, and λ and μ are the Lamé parameters, which depend on the material properties of the propagating media. Typically, in a 2-D or 3-D domain, the free-surface boundary condition aligns with the top plane of our domain, where the vertical traction becomes zero. In our case study, we set both limits of our 1-D domain ($x = 0$ and $x = L$, where L is the length of the array) as free surfaces, $\sigma_{xx}|_{x=0,L} = 0$.

We discretize the domain using two interleaved grids: one holding the stress nodes, and the other holding the velocity nodes, following Levander (1988). This schema, called staggered-grid formulation, is illustrated in Figure 1. To compute the derivatives in space from Equation (1), we apply the fourth-order FD operator to the stress and velocity grids, as follows:

$$\partial_x p_k \approx \frac{c_1 \left(p_{k+\frac{1}{2}} - p_{k-\frac{1}{2}}\right) + c_2 \left(p_{k+\frac{3}{2}} - p_{k-\frac{3}{2}}\right)}{\Delta x} = S_x[p_k]. \tag{2}$$

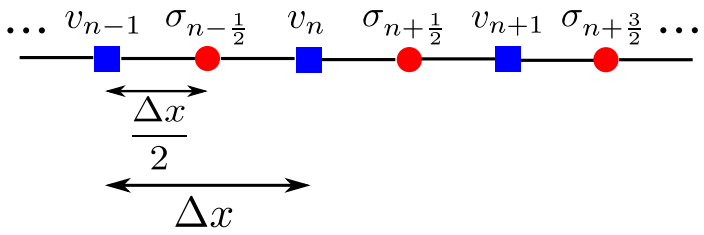

Figure 1: Staggered-grid formulation in a one-dimensional array. Blue nodes hold the velocity values, while red nodes represent stresses. The grid is staggered because stress and velocity nodes are separated by half of the spatial discretization. [**NR**]

S is the *centered* FD stencil operator, p_k is the variable to differentiate at node k (stress or velocity); Δx is the spatial discretization; and c_1 and c_2 are the fourth-order stencil coefficients, ($c_1 = \frac{9}{8}$ and $c_2 = \frac{1}{24}$), as seen in Levander (1988) and Fornberg (1988).

Because there are no nodes beyond the boundaries of the array, we have to resort to *one-sided* stencil operators to update the boundary values. However, one-sided standard FD operators are less precise than their centered counterparts. To preserve the order of accuracy, we employ the MFD operators, following Castillo et al. (2001).

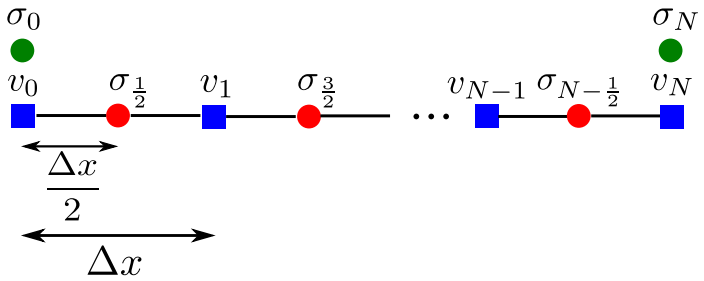

Figure 2: Staggered-grid formulation including the mimetic extra nodes (in green), collocated on the boundary. [**NR**]

The mimetic operators require one extra node to compute the derivative at the boundary. This extra node is collocated on the grid with the boundary node, as illustrated in Figure 2. Velocity nodes are differentiated using the *Mimetic Divergence* operator, G, while stress nodes compute their derivatives using the *Mimetic Gradient* operator D, as explained in de la Puente et al. (2014):

$$\frac{\partial v_x}{\partial x} \approx D[v_x] \qquad \frac{\partial \sigma_{xx}}{\partial x} \approx G[\sigma_{xx}]. \tag{3}$$

Each operator is constructed from three free parameters, α_θ, β_θ, and γ_θ ($\theta = G$ if we are referring to the Gradient operator, $\theta = D$ for the Divergence operator), as introduced by Castillo et al. (2001). These operators have a limited mimetic

bandwidth. When computing derivatives near the boundaries, the coefficients are particular to the mimetic method. As the operator moves to the interior points of the grid, the stencil coefficients become those of the standard FD operator previously discussed. In the specific case of the compact fourth-order operator, the mimetic bandwidth is limited within the first four grid points.

We have a myriad of methods to perform the time integration to retrieve the values of stress and velocity at a certain time step. In general, higher-order methods offer improved precision and reduced dispersion in the wave propagation, but in return require us to either perform more complex calculations or to store more information, such as values at previous time steps, in memory (Moczo and Kristek (2014)). For this study, we use a second-order leapfrog integration. Using this explicit method on Equation (1), and omitting the force term, we obtain the following:

$$\frac{\partial \sigma_{xx}}{\partial x} = \rho \frac{\partial v_x}{\partial t} \approx \rho \frac{v_x^{m+1} - v_x^m}{\Delta t},$$

where Δt represents the time discretization. Finally, using (3)

$$v_x^{m+1} \approx v_x^m + \frac{\Delta t}{\rho}\, G[\sigma_{xx}^m]. \tag{4}$$

Similarly, to update stresses,

$$\sigma_{xx}^{m+\frac{3}{2}} \approx \sigma_{xx}^{m+\frac{1}{2}} + \Delta t\, (\lambda + 2\mu)\, D[v_x^{m+1}]. \tag{5}$$

OPTIMIZING THE MIMETIC OPERATORS

Analyzing the behavior of the MFD operators requires assembling a test to compare different operators and measuring their impact. My test consists of a 1-D domain discretized using a staggered grid, with a free-surface boundary condition at both ends. Instead of using a force term, as seen in Equation (1), I initialize the values in the stress nodes with a Ricker wavelet centered in the domain. Once the simulation begins, the wave propagates both ways in the x direction toward the boundaries located at $x = 0$ and $x = L$, where it is reflected back toward the center of the domain. After several reflections, we reconstruct the wave in the center of the domain by superposition.

If the propagation was modeled analytically, the reconstructed wave should be identical to the initial pulse; as there are no dissipative effects in the problem. However, because of the numerical nature of the simulation, we can expect some errors in phase (numerical dispersion) and some errors in amplitude (numerical dissipation).

To assess the quality of the operators, I consider two criteria: (1) the misfit function and (2) the maximum Courant number of the operator. The misfit function allows us to quantify the dispersion and dissipation error, while the maximum Courant number gives us an idea of how numerically stable the operators are.

The misfit function evaluates the discrepancy between the original and the reconstructed wave in phase and envelope. Less dissipative operators produce results with lower envelope-misfit than their more dissipative counterparts, while operators that are less dispersive produce results with lower phase-misfit.

To estimate how stable the operator is in relation to the others, we turn to its maximum Courant number C_{max}. For a FD simulation to be stable, it is necessary that C, as determined by the grid parameters, is lower than the maximum Courant number allowed by the operator, C_{max}. This necessary condition is referred to as the Courant-Friedrichs-Lewy condition,

$$C = \frac{v_p \, \Delta t}{\Delta x} \leq C_{max}, \tag{6}$$

with v_p representing the maximum P-wave velocity. Therefore, we can use the maximum Courant number of an operator, C_{max}, as a measure of the stability limit in terms of the wave propagation parameters, v_p, Δx, and Δt. For constant discretization and wave velocity of our problem, operators with greater Courant number require fewer iterations to simulate the wave propagation, as larger time steps can be used.

With these testing criteria established, I need to define the optimization problem. The parameter space is every set of α_G, β_G, γ_G, α_D, β_D, and γ_D used to construct an MFD operator. To search for less dispersive operators, I developed a code that explores the parameter space, generating new operators, evaluating them using the test previously defined, and finding those operators that further reduce the misfit function.

The algorithm can be refined for a specific size of the parameter space to explore,

$$\mathcal{P} = [p^{\alpha_G}_{min}, p^{\alpha_G}_{max}] \times [p^{\alpha_D}_{min}, p^{\alpha_D}_{max}] \times \ldots \times [p^{\gamma_D}_{min}, p^{\gamma_D}_{max}], \tag{7}$$

with p_{min}, p_{max} representing the parameter domain limits for each of the six parameters. This space is discretized,

$$\begin{aligned} dp^k &= \frac{p^k_{max} - p^k_{min}}{N} & k &\in \{\alpha_G, \beta_G, \gamma_G, \alpha_D \ldots\} \\ p^k_i &= p^k_{min} + i \cdot dp^k & i &\in \{0, 1, \ldots, N-1, N\}, \end{aligned} \tag{8}$$

and the discrete domain to explore is

$$\mathcal{P}' = \{(p^{\alpha_G}_{i_1}, p^{\beta_G}_{i_2}, p^{\gamma_G}_{i_3}, p^{\alpha_D}_{i_4}, p^{\beta_D}_{i_5}, p^{\gamma_D}_{i_6})\}. \tag{9}$$

Because of the large number of free parameters to consider, the number of solutions to test can be prohibitive: N^6. By choosing $p_{min} = -1$, $p_{max} = 1$ and $N = 20$, which yields a coarse discretization $dp = 0.1$, we need to run the test 64 million times, for more than 40 days of computing time. However, we can reduce the total execution time by taking an iterative approach to the optimization process, and by parallelizing the program.

Instead of solving for the complete parameter space with fine sampling, I adopt an iterative approach. I progressively reduce the limits of the parameter domain, thereby adapting p^k_{min} and p^k_{max} to leave out regions that yield more dispersive or unstable operators to test an increasingly finer discretization. Additionally, I parallelized the code so that it runs simultaneously on multiple computing nodes using *Message Passing Interface* (MPI), each instance running tests on disjoint regions of the parameter space. I also use OpenMP to perform intranode parallelism.

RESULTS

For the purpose of this study, the test case had a fixed P-wave velocity, $v_p = 3000$ m/s, constant spatial discretization $\Delta x = 10$ m, and constant Courant number $C = 0.5$; which yields a temporal discretization of $\Delta t = 1.67$ ms. I propagate the wave for sufficient time for it to reflect against the boundaries on 10 occasions. Using the program previously described with different considerations as to the search direction of the parameter space, I obtain various mimetic operators that merit further analysis. Their attributes, along those of other previously established FD operators are summarized in Table 1.

Operator	Parameters (α_G, β_G, γ_G, α_D, β_D, γ_D)	C_{max}
Taylor	Not applicable (non-mimetic)	0.81
Compact	$(0,\ 0,\ -\frac{1}{24},\ 0,\ 0,\ -\frac{1}{24})$	0.81
Adjoint	$(\frac{142}{3715},\ \frac{-624}{15839},\ \frac{-21}{23707},\ \frac{488}{10121},\ \frac{-367}{7075},\ \frac{-167}{7167})$	0.85
Alpha	$(\frac{-799}{999},\ 0,\ \frac{-21}{23707},\ \frac{233}{999},\ 0,\ \frac{-1}{24})$	0.50
Beta	$(0,\ \frac{-699}{999},\ \frac{-1}{24},\ 0,\ \frac{-227}{999},\ \frac{-1}{24})$	0.64
Optimal	$(\frac{5}{9},\ \frac{-259}{999},\ \frac{-629}{999},\ \frac{2}{9},\ \frac{-1}{9},\ \frac{-370}{999})$	0.68

Table 1: Parameters used to construct each operator and their maximum Courant number.

The *Taylor* operator is a standard one-sided fourth-order FD operator, constructed according to Fornberg (1988). The *Compact* mimetic operator is presented in Castillo et al. (2001) as a fourth-order MFD operator with the smallest mimetic bandwidth possible—one point in the D operator and two points in the G operator. It constitutes our reference when measuring improvement in reducing dispersion with our operators.

The *Adjoint* operator is an approximation of the mimetic operator with a negative adjoint, so that $G \approx -D^T$. This quasi-adjoint MFD operator is presented in Córdova et al. (2016). A benefit of using the quasi-adjoint operator is its increased numerical stability.

The *Alpha* operator is obtained by using our algorithm to search in the α_G and α_D parameter space, keeping the rest with the same values as the *Compact* operator. In similar fashion, we can compose the *Beta* operator by optimizing for the β_G and β_D parameters. Finally, the *Optimal* operator is obtained by searching concurrently for the optimal values of all the parameters.

When considering stability, the MFD operators obtained using our algorithm are more restrictive on the problem parametrization, in order to fulfill Equation (6). The C_{max} of the *Optimal* operator is 16% smaller than that of the more stable *Compact* operator. For comparison, with a constant v_p and Δx, the Δt of the *Optimal* operator needs to be 84% smaller, which results in an increase of 19% in the number of time iterations.

However, our operators outperform the rest when examining the accuracy of the results. Figure 3 illustrates the wave reconstruction. The wave profiles obtained depend on the operator used to model the propagation. The effect on dispersion is apparent in the reconstructed wave, especially for the *Compact* operator.

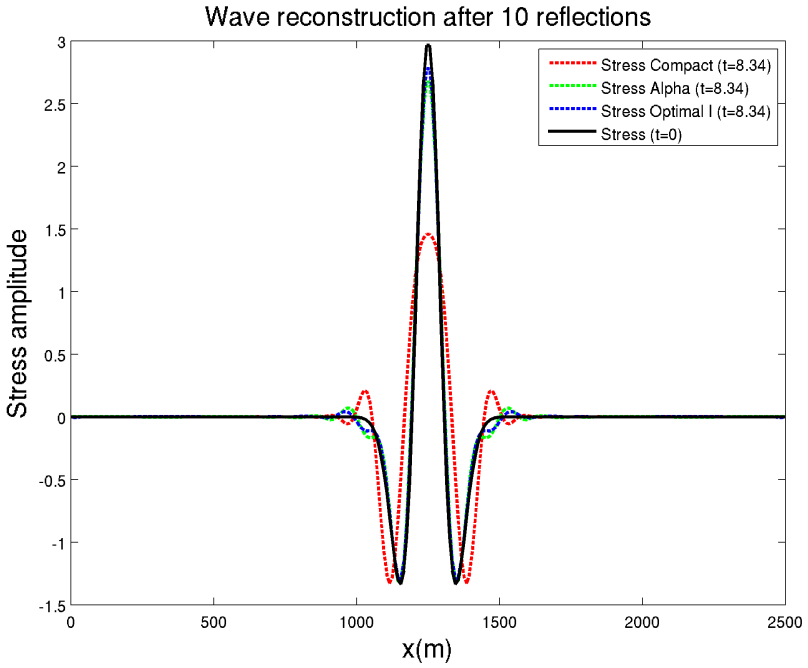

Figure 3: Initial pulse (stress component) and its reconstruction after propagating with different operators. The *Taylor* and *Adjoint* results are omitted, since they are almost indistinguishable from *Compact*. [**NR**]

The effects that each operator has in reducing the dispersion on the test case are

illustrated in Table 2.

Operator	Envelope misfit	Phase misfit
Taylor	43.6%	14.9%
Compact	42.9%	14.9%
Adjoint	42.8%	14.9%
Alpha	8.1%	2.0%
Beta	17.0%	2.8%
Optimal	5.7%	1.1%

Table 2: Envelope and phase misfit results for each operator after propagation in the test case.

Dissipation (on wave envelope) and dispersion (on wave phase) are minimized using our operator, as illustrated by Figures 4 and 5. After 10 reflections, the *Optimal* operator exhibits a 92% decrease in phase misfit and a 87% decrease in envelope misfit. The improved accuracy is preserved as the number of reflections grows, with an 80% and 84% reduction in envelope and phase misfit respectively, at 20 reflections.

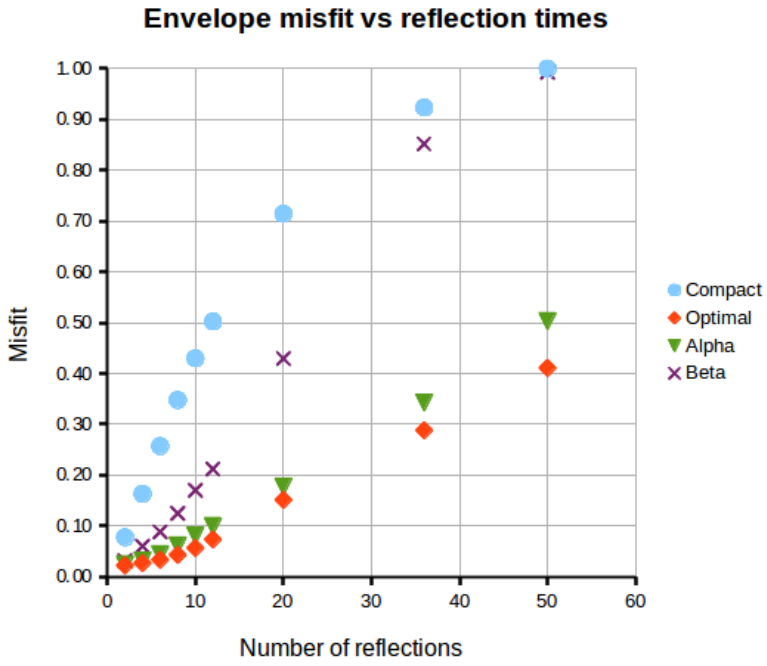

Figure 4: Misfit due to dissipation increases with the number of reflections against the free surface. Operator *Optimal* is less dissipative. [**CR**]

The rate of convergence of an operator with the analytical solution increases as the grid becomes denser. Figure 6 highlights the superior convergence of the *Optimal* operator. It is important to remark that the fourth-order operator requires at least

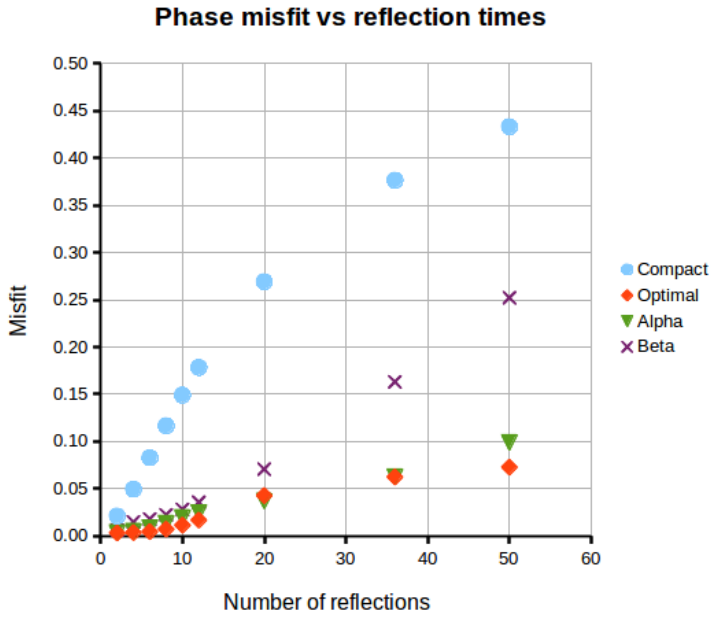

Figure 5: Phase misfit due to dispersion also increases with the number of reflections. Operator *Optimal* outperforms the other operators across the range of reflections. [**CR**]

six points per wavelength to correctly model the wave propagation, as explained in Levander (1988).

DISCUSSION

The MFD method provides alternative operators to the standard FD method. These operators are constructed from a family of six free parameters, and can retain the order of accuracy in the presence of Dirichlet boundary conditions.

Using a parallel scanning algorithm, I searched for sets of parameters to construct MFD operators with reduced dispersion and dissipation effects, on a 1-D medium with free-surface boundary conditions.

The resulting *Optimal* operator outperforms the standard Taylor FD operator and other mimetic operators in reducing wave dispersion and dissipation on the simulation. This increase in numerical accuracy has no impact in the computational cost, because it only requires adjusting the value of the coefficients used to compute the derivative.

There is a trade-off in terms of stability, as the resulting operator is less tolerant to problems with a higher Courant number. Nonetheless, the limits to the stability of the *Optimal* operator are well within typical values used in geophysical applications.

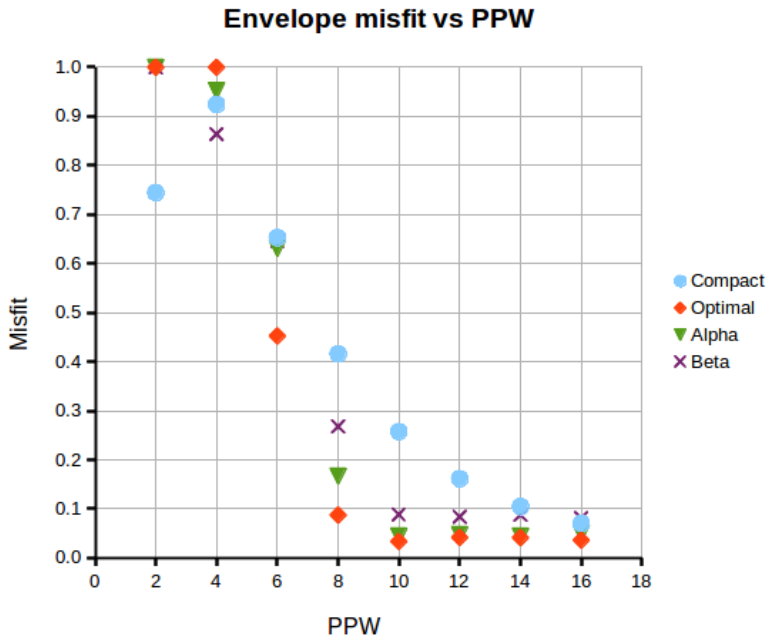

Figure 6: Convergence of the operators as the domain sampling becomes more dense (the number of points per wavelength (PPW) increases). [**CR**]

FUTURE WORK

The optimization of the mimetic operator has successfully been applied to the 1-D case. The 1-D domain has been chosen for its simplicity and inexpensive validation. It remains as future work to find the corresponding operator in 2-D. It should be remarked that the testing methodology will be different, since in a 2-D domain the wave reconstruction and comparison with the initial pulse is not possible, and the analytical solution is difficult to obtain.

The velocity-stress formulation of the elastic wave equation using staggered grids requires two different layouts in the vertical direction: (1) one for which the extra mimetic node on the boundary is a velocity node, and (2) one for which it is a stress node. Because these nodes compute their derivatives with different mimetic operators (D or G), the *Optimal* operator differs between layouts. Thus, the operator obtained by searching for parameters to minimize dispersion in 1-D is not the same as the 2-D case.

Furthermore, it would be of interest to compute the dispersion curves for every operator, both in 1-D and 2-D, as an extra measure to quantify numerical dispersion.

REFERENCES

Castillo, J. E., J. M. Hyman, M. Shashkov, and S. Steinberg, 2001, Fourth and sixth-order conservative finite-difference approximations of the divergence and gradient: Mathematics of Computation, **37**, 171–187.

Córdova, L., O. Rojas, B. Otero, and J. Castillo, 2016, Compact finite difference schemes for the acoustic wave equation: Presented at the 78th EAGE Conference and Exhibition.

de la Puente, J., M. Ferrer, M. Hanzich, J. E. Castillo, and J. M. Cela, 2014, Mimetic seismic wave modeling including topography on deformed staggered grids: Geophysics, **79**, T125–T141.

Fornberg, B., 1988, Generation of finite difference formulas on arbitrarily spaced grids: Mathematics of Computation, **51**, 699–706.

Levander, A. R., 1988, Fourth-order finite-difference P-SV seismograms: Geophysics, **53**, 1425–1436.

Moczo, P. and J. Kristek, 2014, The finite-difference modelling of earthquake motions: Waves and ruptures: Cambridge University Press.